



CERN-EP-2017-248
 LHCb-PAPER-2017-038
 October 5, 2017

Search for dark photons produced in 13 TeV pp collisions

LHCb collaboration[†]

Abstract

Searches are performed for both prompt-like and long-lived dark photons, A' , produced in proton-proton collisions at a center-of-mass energy of 13 TeV, using $A' \rightarrow \mu^+ \mu^-$ decays and a data sample corresponding to an integrated luminosity of 1.6 fb^{-1} collected with the LHCb detector. The prompt-like A' search covers the mass range from near the dimuon threshold up to 70 GeV, while the long-lived A' search is restricted to the low-mass region $214 < m(A') < 350 \text{ MeV}$. No evidence for a signal is found, and 90% confidence level exclusion limits are placed on the γ - A' kinetic-mixing strength. The constraints placed on prompt-like dark photons are the most stringent to date for the mass range $10.6 < m(A') < 70 \text{ GeV}$, and are comparable to the best existing limits for $m(A') < 0.5 \text{ GeV}$. The search for long-lived dark photons is the first to achieve sensitivity using a displaced-vertex signature.

Published in Physical Review Letters **120**, 061801 (2018)

© CERN on behalf of the LHCb collaboration, licence CC-BY-4.0.

[†]Authors are listed at the end of this Letter.

The possibility that dark matter particles may interact via unknown forces, felt only feebly by Standard Model (SM) particles, has motivated substantial effort to search for dark-sector forces (see Ref. [1] for a review). A compelling dark-force scenario involves a massive *dark photon*, A' , whose coupling to the electromagnetic current is suppressed relative to that of the ordinary photon, γ , by a factor of ε . In the minimal model, the dark photon does not couple directly to charged SM particles; however, a coupling may arise via kinetic mixing between the SM hypercharge and A' field strength tensors [2–7]. This mixing provides a potential portal through which dark photons may be produced if kinematically allowed. If the kinetic mixing arises due to processes whose amplitudes involve one or two loops containing high-mass particles, perhaps even at the Planck scale, then $10^{-12} \lesssim \varepsilon^2 \lesssim 10^{-4}$ is expected [1]. Fully exploring this *few-loop* range of kinetic-mixing strength is an important goal of dark-sector physics.

Constraints have been placed on visible A' decays by previous beam-dump [7–21], fixed-target [22–24], collider [25–28], and rare-meson-decay [29–38] experiments. The few-loop region is ruled out for dark photon masses $m(A') \lesssim 10$ MeV ($c = 1$ throughout this Letter). Additionally, the region $\varepsilon^2 \gtrsim 5 \times 10^{-7}$ is excluded for $m(A') < 10.2$ GeV, along with about half of the remaining few-loop region below the dimuon threshold. Many ideas have been proposed to further explore the $[m(A'), \varepsilon^2]$ parameter space [39–51], including an inclusive search for $A' \rightarrow \mu^+ \mu^-$ decays with the LHCb experiment, which is predicted to provide sensitivity to large regions of otherwise inaccessible parameter space using data to be collected during Run 3 of the LHC (2021–2023) [52].

A dark photon produced in proton-proton, pp , collisions via γ - A' mixing inherits the production mechanisms of an off-shell photon with $m(\gamma^*) = m(A')$; therefore, both the production and decay kinematics of the $A' \rightarrow \mu^+ \mu^-$ and $\gamma^* \rightarrow \mu^+ \mu^-$ processes are identical. Furthermore, the expected $A' \rightarrow \mu^+ \mu^-$ signal yield is given by [52]

$$n_{\text{ex}}^{A'}[m(A'), \varepsilon^2] = \varepsilon^2 \left[\frac{n_{\text{ob}}^{\gamma^*}[m(A')]}{2\Delta m} \right] \mathcal{F}[m(A')] \epsilon_{\gamma^*}^{A'}[m(A'), \tau(A')], \quad (1)$$

where $n_{\text{ob}}^{\gamma^*}[m(A')]$ is the observed prompt $\gamma^* \rightarrow \mu^+ \mu^-$ yield in a small $\pm \Delta m$ window around $m(A')$, the function $\mathcal{F}[m(A')]$ includes phase-space and other known factors, and $\epsilon_{\gamma^*}^{A'}[m(A'), \tau(A')]$ is the ratio of the $A' \rightarrow \mu^+ \mu^-$ and $\gamma^* \rightarrow \mu^+ \mu^-$ detection efficiencies, which depends on the A' lifetime, $\tau(A')$. If A' decays to invisible final states are negligible, then $\tau(A') \propto [m(A')\varepsilon^2]^{-1}$ and $A' \rightarrow \mu^+ \mu^-$ decays can potentially be reconstructed as displaced from the primary pp vertex (PV) when the product $m(A')\varepsilon^2$ is small. When $\tau(A')$ is small compared to the experimental resolution, $A' \rightarrow \mu^+ \mu^-$ decays are reconstructed as prompt-like and are experimentally indistinguishable from prompt $\gamma^* \rightarrow \mu^+ \mu^-$ production, resulting in $\epsilon_{\gamma^*}^{A'}[m(A'), \tau(A')] \approx 1$. This facilitates a fully data-driven search and the cancelation of most experimental systematic effects, since the observed $A' \rightarrow \mu^+ \mu^-$ yields, $n_{\text{ob}}^{A'}[m(A')]$, can be normalized to $n_{\text{ex}}^{A'}[m(A'), \varepsilon^2]$ to obtain constraints on ε^2 .

This Letter presents searches for both prompt-like and long-lived dark photons produced in pp collisions at a center-of-mass energy of 13 TeV, using $A' \rightarrow \mu^+ \mu^-$ decays and a data sample corresponding to an integrated luminosity of 1.6 fb^{-1} collected with the LHCb detector in 2016. The prompt-like A' search is performed from near the dimuon threshold up to 70 GeV, above which the $m(\mu^+ \mu^-)$ spectrum is dominated by the Z boson. The long-lived A' search is restricted to the mass range $214 < m(A') < 350$ MeV, where the data sample potentially provides sensitivity.

The LHCb detector is a single-arm forward spectrometer covering the pseudorapidity range $2 < \eta < 5$, described in detail in Refs. [53, 54]. Simulated data samples, which are used to validate the analysis, are produced using the software described in Refs. [55–57]. The online event selection is performed by a trigger [58], which consists of a hardware stage using information from the calorimeter and muon systems, followed by a software stage, which performs a full event reconstruction. At the hardware stage, events are required to have a muon with $p_T \gtrsim 1.8$ GeV, where p_T is the momentum transverse to the beam direction, or a dimuon in which the product of the p_T of each muon is in excess of $(\approx 1.5$ GeV) 2 . The long-lived A' search also uses events selected at the hardware stage independently of the $A' \rightarrow \mu^+ \mu^-$ candidate. In the software stage, $A' \rightarrow \mu^+ \mu^-$ candidates are built from two oppositely charged tracks that form a good quality vertex and satisfy stringent muon-identification criteria. The muons are required to have $2 < \eta < 4.5$, $p_T > 0.5$ (1.0) GeV, momentum $p > 10$ (20) GeV, and be inconsistent (consistent) with originating from the PV in the long-lived (prompt-like) A' search. Finally, the A' candidates are required to satisfy $p_T > 1$ GeV, $2 < \eta < 4.5$, and have a decay topology consistent with originating from the PV.

The prompt-like A' search is based on a data sample where all online-reconstructed particles are stored, but most lower-level information is discarded, greatly reducing the event size. This data-storage strategy, made possible by advances in the LHCb data-taking scheme introduced in 2015 [59, 60], permits the recording of all events that contain a prompt-like dimuon candidate without placing any requirements on $m(\mu^+ \mu^-)$. The $m(\mu^+ \mu^-)$ spectrum recorded by the trigger is provided in the Supplemental Material to this Letter [61].

Three main types of background contribute to the prompt-like A' search: prompt $\gamma^* \rightarrow \mu^+ \mu^-$ production, which is irreducible; resonant decays to $\mu^+ \mu^-$, whose mass-peak regions are avoided in the search; and various types of misreconstruction. The misreconstruction background consists of three dominant contributions: double misidentification of prompt hadrons as muons, hh ; a misidentified prompt hadron combined with a muon produced in a decay of a hadron containing a heavy-flavor quark, Q , where the muon is misreconstructed as prompt-like, $h\mu_Q$; and the misreconstruction of two muons produced in Q -hadron decays, $\mu_Q \mu_Q$. These backgrounds are highly suppressed by the stringent muon-identification and prompt-like requirements applied in the trigger; however, in the region $[m(\phi), m(\Upsilon)]$, the misreconstructed backgrounds overwhelm the signal-like $\gamma^* \rightarrow \mu^+ \mu^-$ contribution.

For masses below (above) the ϕ meson mass, dark photons are expected to be predominantly produced in meson-decay (Drell-Yan) processes in pp collisions at LHCb. A well-known signature of Drell-Yan production is dimuons that are largely isolated, and a high-mass dark photon would inherit this property. The signal sensitivity is enhanced by applying a jet-based isolation requirement for $m(A') > m(\phi)$, which improves the sensitivity by up to a factor of two at low masses and by $\mathcal{O}(10\%)$ for $m(A') > 10$ GeV. Jet reconstruction is performed by clustering charged and neutral particle-flow candidates [62] using the anti- k_T clustering algorithm [63] with $R = 0.5$ as implemented in FASTJET [64]. Muons with $p_T(\mu)/p_T(\text{jet}) < 0.7$ are rejected, where the contribution to $p_T(\text{jet})$ from the other muon is excluded if both muons are clustered in the same jet, as this is found to provide nearly optimal sensitivity for all $m(A') > m(\phi)$. Figure 1 shows the resulting prompt-like $m(\mu^+ \mu^-)$ spectrum using Δm bins that are $\sigma[m(\mu^+ \mu^-)]/2$ wide, where $\sigma[m(\mu^+ \mu^-)]$ is the mass resolution which varies from about 0.7 MeV near threshold

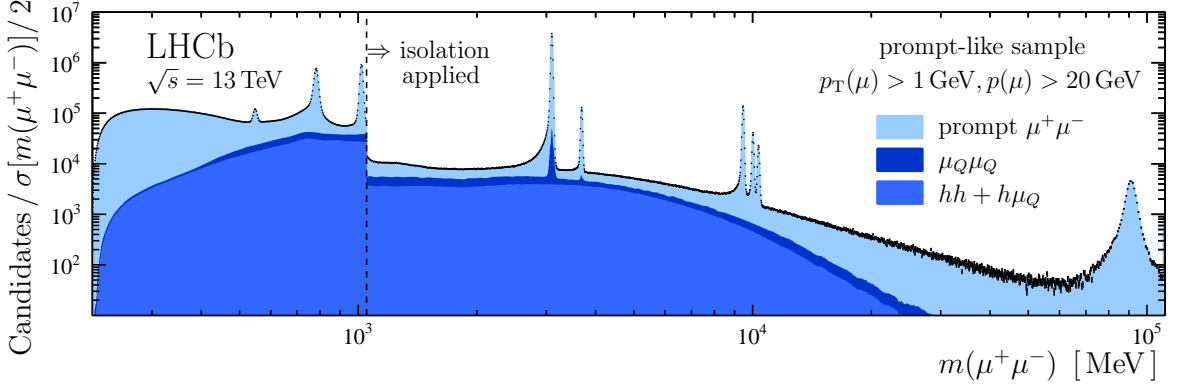


Figure 1: Prompt-like mass spectrum, where the categorization of the data as prompt $\mu^+\mu^-$, $\mu_Q\mu_Q$, and $hh + h\mu_Q$ is determined using the fits described in the text.

to 0.7 GeV at $m(\mu^+\mu^-) = 70$ GeV.

The prompt-like A' search strategy involves determining the observed $A' \rightarrow \mu^+\mu^-$ yields from fits to the $m(\mu^+\mu^-)$ spectrum, and normalizing them using Eq. 1 to obtain constraints on ε^2 . To determine $n_{\text{ob}}^{\gamma^*}[m(A')]$ for use in Eq. 1, binned extended maximum likelihood fits are performed using the dimuon vertex-fit quality, $\chi_{\text{VF}}^2(\mu^+\mu^-)$, and $\min[\chi_{\text{IP}}^2(\mu^\pm)]$ distributions, where $\chi_{\text{IP}}^2(\mu)$ is defined as the difference in $\chi_{\text{VF}}^2(\text{PV})$ when the PV is reconstructed with and without the muon track. The $\chi_{\text{VF}}^2(\mu^+\mu^-)$ and $\min[\chi_{\text{IP}}^2(\mu^\pm)]$ fits are performed independently at each mass, with the mean of the $n_{\text{ob}}^{\gamma^*}[m(A')]$ results used as the nominal value and half the difference assigned as a systematic uncertainty.

Both fit quantities are built from features that approximately follow χ^2 probability density functions (PDFs) with minimal mass dependence. The prompt-dimuon PDFs are taken directly from data at $m(J/\psi)$ and $m(Z)$, where prompt resonances are dominant (see Fig. 1). Small p_T -dependent corrections are applied to obtain the PDFs at all other masses. These PDFs are validated near threshold, at $m(\phi)$, and at $m(\Upsilon(1S))$, where the data predominantly consist of prompt dimuons. The sum of the hh and $h\mu_Q$ contributions, which each involve misidentified prompt hadrons, is determined using same-sign $\mu^\pm\mu^\pm$ candidates that satisfy all of the prompt-like criteria. A correction is applied to the observed $\mu^\pm\mu^\pm$ yield at each mass to account for the difference in the production rates of $\pi^+\pi^-$ and $\pi^\pm\pi^\pm$, since double misidentified $\pi^+\pi^-$ pairs are the dominant source of the hh background. This correction, which is derived using a prompt-like dipion data sample weighted by p_T -dependent muon-misidentification probabilities, is as large as a factor of two near $m(\rho)$ but negligible for $m(\mu^+\mu^-) \gtrsim 2$ GeV. The PDFs for the $\mu_Q\mu_Q$ background, which involves muon pairs produced in Q -hadron decays that occur displaced from the PV, are obtained from simulation. These muons are rarely produced at the same spatial point unless the decay chain involves charmonium. Example $\min[\chi_{\text{IP}}^2(\mu^\pm)]$ fit results are provided in Ref. [61], while Fig. 1 shows the resulting data categorizations. Finally, the $n_{\text{ob}}^{\gamma^*}[m(A')]$ yields are corrected for bin migration due to bremsstrahlung, and the small expected Bethe-Heitler contribution is subtracted [52].

The prompt-like mass spectrum is scanned in steps of $\sigma[m(\mu^+\mu^-)]/2$ searching for $A' \rightarrow \mu^+\mu^-$ contributions. At each mass, a binned extended maximum likelihood fit is performed using all prompt-like candidates in a $\pm 12.5\sigma[m(\mu^+\mu^-)]$ window around $m(A')$. The profile likelihood is used to determine the p -value and the confidence interval for

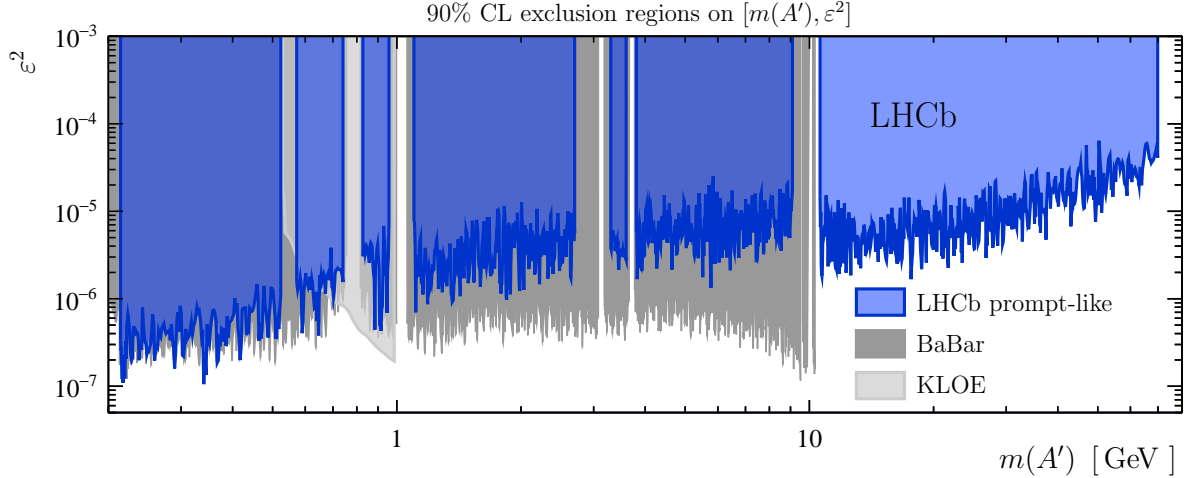


Figure 2: Regions of the $[m(A'), \varepsilon^2]$ parameter space excluded at 90% CL by the prompt-like A' search compared to the best existing limits [27, 38].

$n_{\text{ob}}^{A'}[m(A')]$, from which an upper limit at 90% confidence level (CL) is obtained. The signal PDFs are determined using a combination of simulated $A' \rightarrow \mu^+ \mu^-$ decays and the widths of the large resonance peaks observed in the data. The strategy proposed in Ref. [65] is used to select the background model and assign its uncertainty. This method takes as input a large set of potential background components, which here includes all Legendre modes up to tenth order and dedicated terms for known resonances, and then performs a data-driven model-selection process whose uncertainty is included in the profile likelihood following Ref. [66]. More details about the fits, including discussion on peaking backgrounds, are provided in Ref. [61]. The most significant excess is 3.3σ at $m(A') \approx 5.8$ GeV, corresponding to a p -value of 38% after accounting for the trials factor due to the number of prompt-like signal hypotheses.

Regions of the $[m(A'), \varepsilon^2]$ parameter space where the upper limit on $n_{\text{ob}}^{A'}[m(A')]$ is less than $n_{\text{ex}}^{A'}[m(A'), \varepsilon^2]$ are excluded at 90% CL. Figure 2 shows that the constraints placed on prompt-like dark photons are comparable to the best existing limits below 0.5 GeV, and are the most stringent for $10.6 < m(A') < 70$ GeV. In the latter mass range, a nonnegligible model-dependent mixing with the Z boson introduces additional kinetic-mixing parameters altering Eq. 1; however, the expanded A' model space is highly constrained by precision electroweak measurements. This search adopts the parameter values suggested in Refs. [67, 68]. The LHCb detector response is found to be independent of which quark-annihilation process produces the dark photon above 10 GeV, making it easy to recast the results in Fig. 2 for other models.

For the long-lived dark photon search, the stringent criteria applied in the trigger make contamination from prompt muon candidates negligible. The dominant background contributions to the long-lived A' search are as follows: photon conversions to $\mu^+ \mu^-$ in the silicon-strip vertex detector (the VELO) that surrounds the pp interaction region [69]; b -hadron decays where two muons are produced in the decay chain; and the low-mass tail from $K_s^0 \rightarrow \pi^+ \pi^-$ decays, where both pions are misidentified as muons. Additional sources of background are negligible, *e.g.* kaon and hyperon decays, and Q -hadron decays producing a muon and a hadron that is misidentified as a muon.

Photon conversions in the VELO dominate the long-lived data sample at low masses. A

new method, which is described in detail in Ref. [70], was recently developed for identifying particles created in secondary interactions with the VELO material. A high-precision three-dimensional material map was produced from a data sample of secondary hadronic interactions. Using this material map, along with properties of the $A' \rightarrow \mu^+ \mu^-$ decay vertex and muon tracks, a p -value is assigned to the photon-conversion hypothesis for each long-lived $A' \rightarrow \mu^+ \mu^-$ candidate. A mass-dependent requirement is applied to these p -values that reduces the expected photon-conversion yields to a negligible level.

A characteristic signature of muons produced in b -hadron decays is the presence of additional displaced tracks. Events are rejected if they are selected by the inclusive Q -hadron software trigger [71] independently of the presence of the $A' \rightarrow \mu^+ \mu^-$ candidate. Furthermore, two boosted decision tree (BDT) classifiers, originally developed for studying $B_{(s)}^0 \rightarrow \mu^+ \mu^-$ decays [72], are used to identify other tracks in the event that are consistent with having originated from the same b -hadron decay as the signal muon candidates. The requirements placed on the BDT responses, which are optimized using a data sample of K_s^0 decays as a signal proxy, reject 70% of the b -hadron background at a cost of about 10% loss in signal efficiency.

As in the prompt-like A' search, the normalization is based on Eq. 1; however, in the long-lived A' search, $\epsilon_{\gamma^*}^{A'}[m(A'), \tau(A')]$ is not unity, in part because the efficiency depends on the decay time, t . Furthermore, the looser kinematic, muon-identification, and hardware-trigger requirements applied to long-lived $A' \rightarrow \mu^+ \mu^-$ candidates, *cf.* prompt-like candidates, increase the efficiency by a factor of 7 to 10, ignoring t -dependent effects. These $m(A')$ -dependent factors are determined using a small control data sample of dimuon candidates consistent with originating from the PV, but otherwise satisfying the long-lived criteria. A relative 10% systematic uncertainty is assigned to the long-lived $A' \rightarrow \mu^+ \mu^-$ normalization due to background contamination in the control sample.

The fact that the kinematics are identical for $A' \rightarrow \mu^+ \mu^-$ and prompt $\gamma^* \rightarrow \mu^+ \mu^-$ decays for $m(A') = m(\gamma^*)$ enables the t dependence of the signal efficiency to be determined using a data-driven approach. For each value of $[m(A'), \tau(A')]$, prompt $\gamma^* \rightarrow \mu^+ \mu^-$ candidates in the control data sample near $m(A')$ are resampled many times as long-lived $A' \rightarrow \mu^+ \mu^-$ decays, and all t -dependent properties, *e.g.* $\min[\chi_{\text{IP}}^2(\mu^\pm)]$, are recalculated based on the resampled decay-vertex locations. This approach is validated in simulation by using prompt $A' \rightarrow \mu^+ \mu^-$ decays to predict the properties of long-lived $A' \rightarrow \mu^+ \mu^-$ decays, and based on these studies a 2% systematic uncertainty is assigned to the signal efficiencies. The $\epsilon_{\gamma^*}^{A'}[m(A'), \tau(A')]$ values integrated over t are provided in Ref. [61].

A scan is again performed in discrete steps of $\sigma[m(\mu^+ \mu^-)]/2$ looking for $A' \rightarrow \mu^+ \mu^-$ contributions; however, in this case, discrete steps in $\tau(A')$ are also considered. Binned extended maximum likelihood fits are performed using all long-lived candidates and the three-dimensional feature space of $m(\mu^+ \mu^-)$, t , and the consistency of the decay topology as quantified in the decay-fit χ_{DF}^2 , which has three degrees of freedom (the data distribution is provided in Ref. [61]). The expected conversion contribution is derived in each bin from the number of candidates rejected by the conversion criterion. Two large control data samples are used to develop and validate the modeling of the b -hadron and K_s^0 contributions: candidates that fail the b -hadron suppression requirements, and candidates that fail but nearly satisfy the muon-identification requirements. The profile likelihood is used to obtain the p -values and confidence intervals on $n_{\text{ob}}^{A'}[m(A'), \tau(A')]$. The most significant excess occurs at $m(A') = 239$ MeV and $\tau(A') = 0.86$ ps, where the p -value corresponds to 3.0σ . Considering only the long-lived-search trials factor reduces this to

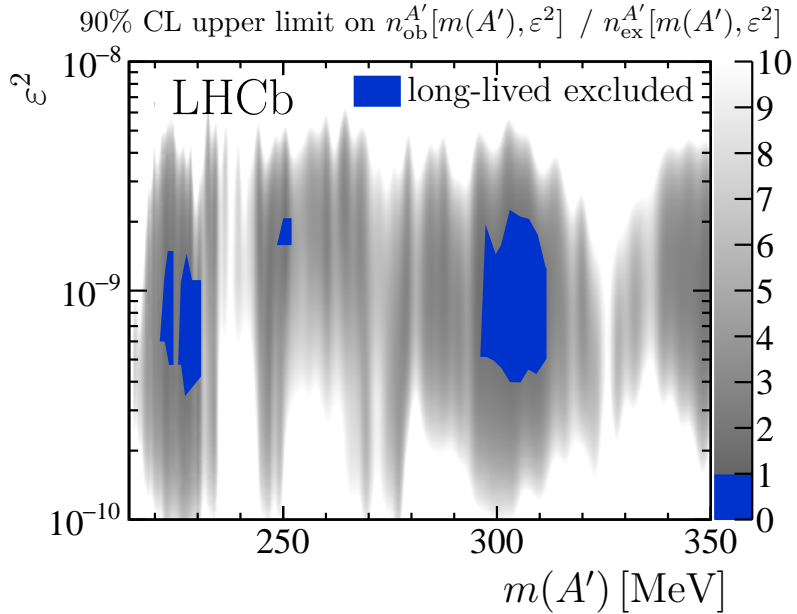


Figure 3: Ratio of the observed upper limit on $n_{\text{ob}}^{A'}[m(A'), \varepsilon^2]$ at 90% CL to its expected value, where regions less than unity are excluded. There are no constraints from previous experiments in this region.

2.0σ . More details about these fits are provided in Ref. [61].

Under the assumption that A' decays to invisible final states are negligible, there is a fixed (and known) relationship between $\tau(A')$ and ε^2 at each mass [52]; therefore, the upper limits on $n_{\text{ob}}^{A'}[m(A'), \tau(A')]$ can be translated into limits on $n_{\text{ob}}^{A'}[m(A'), \varepsilon^2]$. Regions of the $[m(A'), \varepsilon^2]$ parameter space where the upper limit on $n_{\text{ob}}^{A'}[m(A'), \varepsilon^2]$ is less than $n_{\text{ex}}^{A'}[m(A'), \varepsilon^2]$ are excluded at 90% CL (see Fig. 3). While only small regions of $[m(A'), \varepsilon^2]$ space are excluded, a sizable portion of this parameter space will soon become accessible as more data are collected.

In summary, searches are performed for both prompt-like and long-lived dark photons produced in pp collisions at a center-of-mass energy of 13 TeV, using $A' \rightarrow \mu^+ \mu^-$ decays and a data sample corresponding to an integrated luminosity of 1.6 fb^{-1} collected with the LHCb detector during 2016. The prompt-like A' search covers the mass range from near the dimuon threshold up to 70 GeV, while the long-lived A' search is restricted to the low-mass region $214 < m(A') < 350 \text{ MeV}$. No evidence for a signal is found, and 90% CL exclusion regions are set on the $\gamma-A'$ kinetic-mixing strength. The constraints placed on prompt-like dark photons are the most stringent to date for the mass range $10.6 < m(A') < 70 \text{ GeV}$, and are comparable to the best existing limits for $m(A') < 0.5 \text{ GeV}$. The search for long-lived dark photons is the first to achieve sensitivity using a displaced-vertex signature.

These results demonstrate the unique sensitivity of the LHCb experiment to dark photons, even using a data sample collected with a trigger that is inefficient for low-mass $A' \rightarrow \mu^+ \mu^-$ decays. Using knowledge gained from this analysis, the software-trigger efficiency for low-mass dark photons has been significantly improved for 2017 data taking. Looking forward to Run 3, the planned increase in luminosity and removal of the hardware-trigger stage should increase the number of expected $A' \rightarrow \mu^+ \mu^-$ decays in the low-mass region by a factor of $\mathcal{O}(100-1000)$ compared to the 2016 data sample.

Acknowledgements

We express our gratitude to our colleagues in the CERN accelerator departments for the excellent performance of the LHC. We thank the technical and administrative staff at the LHCb institutes. We acknowledge support from CERN and from the national agencies: CAPES, CNPq, FAPERJ and FINEP (Brazil); MOST and NSFC (China); CNRS/IN2P3 (France); BMBF, DFG and MPG (Germany); INFN (Italy); NWO (The Netherlands); MNiSW and NCN (Poland); MEN/IFA (Romania); MinES and FASO (Russia); MinECo (Spain); SNSF and SER (Switzerland); NASU (Ukraine); STFC (United Kingdom); NSF (USA). We acknowledge the computing resources that are provided by CERN, IN2P3 (France), KIT and DESY (Germany), INFN (Italy), SURF (The Netherlands), PIC (Spain), GridPP (United Kingdom), RRCKI and Yandex LLC (Russia), CSCS (Switzerland), IFIN-HH (Romania), CBPF (Brazil), PL-GRID (Poland) and OSC (USA). We are indebted to the communities behind the multiple open-source software packages on which we depend. Individual groups or members have received support from AvH Foundation (Germany), EPLANET, Marie Skłodowska-Curie Actions and ERC (European Union), ANR, Labex P2IO, ENIGMASS and OCEVU, and Région Auvergne-Rhône-Alpes (France), RFBR and Yandex LLC (Russia), GVA, XuntaGal and GENCAT (Spain), Herchel Smith Fund, the Royal Society, the English-Speaking Union and the Leverhulme Trust (United Kingdom).

References

- [1] J. Alexander *et al.*, *Dark Sectors 2016 Workshop: Community Report*, 2016. [arXiv:1608.08632](https://arxiv.org/abs/1608.08632).
- [2] L. B. Okun, *Limits of electrodynamcis: Paraphotons?*, Sov. Phys. JETP **56** (1982) 502, [Zh. Eksp. Teor. Fiz. **83** (1982) 892].
- [3] P. Galison and A. Manohar, *Two Z's or not two Z's?*, Phys. Lett. **B136** (1984) 279.
- [4] B. Holdom, *Two U(1)'s and ϵ charge shifts*, Phys. Lett. **B166** (1986) 196.
- [5] M. Pospelov, A. Ritz, and M. B. Voloshin, *Secluded WIMP dark matter*, Phys. Lett. **B662** (2008) 53, [arXiv:0711.4866](https://arxiv.org/abs/0711.4866).
- [6] N. Arkani-Hamed, D. P. Finkbeiner, T. R. Slatyer, and N. Weiner, *A theory of dark matter*, Phys. Rev. **D79** (2009) 015014, [arXiv:0810.0713](https://arxiv.org/abs/0810.0713).
- [7] J. D. Bjorken, R. Essig, P. Schuster, and N. Toro, *New fixed-target experiments to search for dark gauge forces*, Phys. Rev. **D80** (2009) 075018, [arXiv:0906.0580](https://arxiv.org/abs/0906.0580).
- [8] CHARM collaboration, F. Bergsma *et al.*, *A search for decays of heavy neutrinos in the mass range 0.5 GeV to 2.8 GeV*, Phys. Lett. **B166** (1986) 473.
- [9] A. Konaka *et al.*, *Search for neutral particles in electron-beam-dump experiment*, Phys. Rev. Lett. **57** (1986) 659.
- [10] E. M. Riordan *et al.*, *Search for short-lived axions in an electron-beam-dump experiment*, Phys. Rev. Lett. **59** (1987) 755.

- [11] J. D. Bjorken, S. Ecklund, W. R. Nelson, A. Abashian, C. Church, B. Lu, L. W. Mo, T. A. Nunamaker, and P. Rassmann, *Search for neutral metastable penetrating particles produced in the SLAC beam dump*, Phys. Rev. **D38** (1988) 3375.
- [12] A. Bross, M. Crisler, S. H. Pordes, J. Volk, S. Errede, and J. Wrbanek, *A search for short-lived particles produced in an electron beam dump*, Phys. Rev. Lett. **67** (1991) 2942.
- [13] M. Davier and H. Nguyen Ngoc, *An unambiguous search for a light Higgs boson*, Phys. Lett. **B229** (1989) 150.
- [14] LSND collaboration, C. Athanassopoulos *et al.*, *Evidence for $\nu_\mu \rightarrow \nu_e$ oscillations from pion decay in flight neutrinos*, Phys. Rev. **C58** (1998) 2489, [arXiv:nucl-ex/9706006](https://arxiv.org/abs/nucl-ex/9706006).
- [15] NOMAD collaboration, P. Astier *et al.*, *Search for heavy neutrinos mixing with tau neutrinos*, Phys. Lett. **B506** (2001) 27, [arXiv:hep-ex/0101041](https://arxiv.org/abs/hep-ex/0101041).
- [16] E787 collaboration, S. Adler *et al.*, *Further search for the decay $K^+ \rightarrow \pi^+ \nu \bar{\nu}$ in the momentum region $p < 195$ MeV/c*, Phys. Rev. **D70** (2004) 037102, [arXiv:hep-ex/0403034](https://arxiv.org/abs/hep-ex/0403034).
- [17] BNL-E949 collaboration, A. V. Artamonov *et al.*, *Study of the decay $K^+ \rightarrow \pi^+ \nu \bar{\nu}$ in the momentum region $140 < P_\pi < 199$ MeV/c*, Phys. Rev. **D79** (2009) 092004, [arXiv:0903.0030](https://arxiv.org/abs/0903.0030).
- [18] R. Essig, R. Harnik, J. Kaplan, and N. Toro, *Discovering new light states at neutrino experiments*, Phys. Rev. **D82** (2010) 113008, [arXiv:1008.0636](https://arxiv.org/abs/1008.0636).
- [19] J. Blümlein and J. Brunner, *New exclusion limits for dark gauge forces from beam-dump data*, Phys. Lett. **B701** (2011) 155, [arXiv:1104.2747](https://arxiv.org/abs/1104.2747).
- [20] S. N. Glinenko, *Constraints on sub-GeV hidden sector gauge bosons from a search for heavy neutrino decays*, Phys. Lett. **B713** (2012) 244, [arXiv:1204.3583](https://arxiv.org/abs/1204.3583).
- [21] J. Blümlein and J. Brunner, *New exclusion limits on dark gauge forces from proton bremsstrahlung in beam-dump data*, Phys. Lett. **B731** (2014) 320, [arXiv:1311.3870](https://arxiv.org/abs/1311.3870).
- [22] APEX collaboration, S. Abrahamyan *et al.*, *Search for a new gauge boson in electron-nucleus fixed-target scattering by the APEX experiment*, Phys. Rev. Lett. **107** (2011) 191804, [arXiv:1108.2750](https://arxiv.org/abs/1108.2750).
- [23] A1 collaboration, H. Merkel *et al.*, *Search at the Mainz Microtron for light massive gauge bosons relevant for the muon g-2 anomaly*, Phys. Rev. Lett. **112** (2014) 221802, [arXiv:1404.5502](https://arxiv.org/abs/1404.5502).
- [24] A1 collaboration, H. Merkel *et al.*, *Search for light gauge bosons of the dark sector at the Mainz Microtron*, Phys. Rev. Lett. **106** (2011) 251802, [arXiv:1101.4091](https://arxiv.org/abs/1101.4091).
- [25] BaBar collaboration, B. Aubert *et al.*, *Search for dimuon decays of a light scalar boson in radiative transitions $\Upsilon \rightarrow \gamma A^0$* , Phys. Rev. Lett. **103** (2009) 081803, [arXiv:0905.4539](https://arxiv.org/abs/0905.4539).

- [26] D. Curtin *et al.*, *Exotic decays of the 125 GeV Higgs boson*, Phys. Rev. **D90** (2014) 075004, [arXiv:1312.4992](#).
- [27] BaBar collaboration, J. P. Lees *et al.*, *Search for a dark photon in e^+e^- collisions at BaBar*, Phys. Rev. Lett. **113** (2014) 201801, [arXiv:1406.2980](#).
- [28] BESIII collaboration, M. Ablikim *et al.*, *Dark photon search in the mass range between 1.5 and 3.4 GeV/c²*, [arXiv:1705.04265](#).
- [29] G. Bernardi *et al.*, *Search for neutrino decay*, Phys. Lett. **B166** (1986) 479.
- [30] SINDRUM I collaboration, R. Meijer Drees *et al.*, *Search for weakly interacting neutral bosons produced in π^-p interactions at rest and decaying into e^+e^- pairs*, Phys. Rev. Lett. **68** (1992) 3845.
- [31] KLOE-2 collaboration, F. Archilli *et al.*, *Search for a vector gauge boson in ϕ meson decays with the KLOE detector*, Phys. Lett. **B706** (2012) 251, [arXiv:1110.0411](#).
- [32] S. N. Gninenko, *Stringent limits on the $\pi^0 \rightarrow \gamma X, X \rightarrow e^+e^-$ decay from neutrino experiments and constraints on new light gauge bosons*, Phys. Rev. **D85** (2012) 055027, [arXiv:1112.5438](#).
- [33] KLOE-2 collaboration, D. Babusci *et al.*, *Limit on the production of a light vector gauge boson in ϕ meson decays with the KLOE detector*, Phys. Lett. **B720** (2013) 111, [arXiv:1210.3927](#).
- [34] WASA-at-COSY collaboration, P. Adlarson *et al.*, *Search for a dark photon in the $\pi^0 \rightarrow e^+e^-\gamma$ decay*, Phys. Lett. **B726** (2013) 187, [arXiv:1304.0671](#).
- [35] HADES collaboration, G. Agakishiev *et al.*, *Searching a dark photon with HADES*, Phys. Lett. **B731** (2014) 265, [arXiv:1311.0216](#).
- [36] PHENIX collaboration, A. Adare *et al.*, *Search for dark photons from neutral meson decays in pp and dAu collisions at $\sqrt{s_{NN}} = 200$ GeV*, Phys. Rev. **C91** (2015) 031901, [arXiv:1409.0851](#).
- [37] NA48/2 collaboration, J. R. Batley *et al.*, *Search for the dark photon in π^0 decays*, Phys. Lett. **B746** (2015) 178, [arXiv:1504.00607](#).
- [38] KLOE-2 collaboration, A. Anastasi *et al.*, *Limit on the production of a new vector boson in $e^+e^- \rightarrow U\gamma, U \rightarrow \pi^+\pi^-$ with the KLOE experiment*, Phys. Lett. **B757** (2016) 356, [arXiv:1603.06086](#).
- [39] R. Essig, P. Schuster, N. Toro, and B. Wojtsekhowski, *An electron fixed target experiment to search for a new vector boson A' decaying to e^+e^-* , JHEP **02** (2011) 009, [arXiv:1001.2557](#).
- [40] M. Freytsis, G. Ovanesyan, and J. Thaler, *Dark force detection in low energy ep collisions*, JHEP **01** (2010) 111, [arXiv:0909.2862](#).
- [41] J. Balewski *et al.*, *DarkLight: A search for dark forces at the Jefferson Laboratory Free-Electron Laser facility*, [arXiv:1307.4432](#).

- [42] B. Wojtsekhowski, D. Nikolenko, and I. Racheck, *Searching for a new force at VEPP-3*, arXiv:1207.5089.
- [43] T. Beranek, H. Merkel, and M. Vanderhaeghen, *Theoretical framework to analyze searches for hidden light gauge bosons in electron scattering fixed target experiments*, Phys. Rev. **D88** (2013) 015032, arXiv:1303.2540.
- [44] B. Echenard, R. Essig, and Y.-M. Zhong, *Projections for dark photon searches at Mu3e*, JHEP **01** (2015) 113, arXiv:1411.1770.
- [45] M. Battaglieri *et al.*, *The Heavy Photon Search test detector*, Nucl. Instrum. Meth. **A777** (2015) 91, arXiv:1406.6115.
- [46] S. Alekhin *et al.*, *A facility to Search for Hidden Particles at the CERN SPS: the SHiP physics case*, arXiv:1504.04855.
- [47] S. Gardner, R. J. Holt, and A. S. Tadepalli, *New prospects in fixed target searches for dark forces with the SeaQuest experiment at Fermilab*, Phys. Rev. **D93** (2016) 115015, arXiv:1509.00050.
- [48] P. Ilten, J. Thaler, M. Williams, and W. Xue, *Dark photons from charm mesons at LHCb*, Phys. Rev. **D92** (2015) 115017, arXiv:1509.06765.
- [49] D. Curtin, R. Essig, S. Gori, and J. Shelton, *Illuminating dark photons with high-energy colliders*, JHEP **02** (2015) 157, arXiv:1412.0018.
- [50] M. He, X.-G. He, and C.-K. Huang, *Dark photon search at a circular e^+e^- collider*, Int. J. Mod. Phys. **A32** (2017) 1750138, arXiv:1701.08614.
- [51] J. Kozaczuk, *Dark photons from nuclear transitions*, arXiv:1708.06349.
- [52] P. Ilten, Y. Soreq, J. Thaler, M. Williams, and W. Xue, *Proposed inclusive dark photon search at LHCb*, Phys. Rev. Lett. **116** (2016) 251803, arXiv:1603.08926.
- [53] LHCb collaboration, A. A. Alves Jr. *et al.*, *The LHCb detector at the LHC*, JINST **3** (2008) S08005.
- [54] LHCb collaboration, R. Aaij *et al.*, *LHCb detector performance*, Int. J. Mod. Phys. **A30** (2015) 1530022, arXiv:1412.6352.
- [55] T. Sjöstrand, S. Ask, J. R. Christiansen, R. Corke, N. Desai, P. Ilten, S. Mrenna, S. Prestel, C. O. Rasmussen, and P. Z. Skands, *An Introduction to PYTHIA 8.2*, Comput. Phys. Commun. **191** (2015) 159, arXiv:1410.3012; T. Sjöstrand, S. Mrenna, and P. Skands, *A brief introduction to PYTHIA 8.1*, Comput. Phys. Commun. **178** (2008) 852, arXiv:0710.3820.
- [56] I. Belyaev *et al.*, *Handling of the generation of primary events in Gauss, the LHCb simulation framework*, J. Phys. Conf. Ser. **331** (2011) 032047.
- [57] Geant4 collaboration, J. Allison *et al.*, *Geant4 developments and applications*, IEEE Trans. Nucl. Sci. **53** (2006) 270; Geant4 collaboration, S. Agostinelli *et al.*, *Geant4: A simulation toolkit*, Nucl. Instrum. Meth. **A506** (2003) 250.

- [58] R. Aaij *et al.*, *The LHCb trigger and its performance in 2011*, JINST **8** (2013) P04022, [arXiv:1211.3055](#).
- [59] G. Dujany and B. Storaci, *Real-time alignment and calibration of the LHCb Detector in Run II*, J. Phys. Conf. Ser. **664** (2015) 082010.
- [60] R. Aaij *et al.*, *Tesla: An application for real-time data analysis in high energy physics*, Comput. Phys. Commun. **208** (2016) 35, [arXiv:1604.05596](#).
- [61] See Supplemental Material to this Letter for additional fit details and figures.
- [62] LHCb collaboration, R. Aaij *et al.*, *Study of forward $Z + \text{jet}$ production in pp collisions at $\sqrt{s} = 7 \text{ TeV}$* , JHEP **01** (2014) 033, [arXiv:1310.8197](#).
- [63] M. Cacciari, G. P. Salam, and G. Soyez, *The anti- k_T jet clustering algorithm*, JHEP **0804** (2008) 063, [arXiv:0802.1189](#).
- [64] M. Cacciari, G. P. Salam, and G. Soyez, *FastJet user manual*, Eur. Phys. J. **C72** (2012) 1896, [arXiv:1111.6097](#).
- [65] M. Williams, *A novel approach to the bias-variance problem in bump hunting*, JINST **12** (2017) P09034, [arXiv:1705.03578](#).
- [66] P. D. Dauncey, M. Kenzie, N. Wardle, and G. J. Davies, *Handling uncertainties in background shapes*, JINST **10** (2015) P04015, [arXiv:1408.6865](#).
- [67] S. Cassel, D. M. Ghilencea, and G. G. Ross, *Electroweak and dark matter constraints on a Z' in models with a hidden valley*, Nucl. Phys. **B827** (2010) 256, [arXiv:0903.1118](#).
- [68] J. M. Cline, G. Dupuis, Z. Liu, and W. Xue, *The windows for kinetically mixed Z' -mediated dark matter and the galactic center gamma ray excess*, JHEP **08** (2014) 131, [arXiv:1405.7691](#).
- [69] R. Aaij *et al.*, *Performance of the LHCb Vertex Locator*, JINST **9** (2014) P09007, [arXiv:1405.7808](#).
- [70] *Mapping the material in the LHCb vertex locator using secondary hadronic interactions*, in preparation.
- [71] T. Likhomanenko, P. Ilten, E. Khairullin, A. Rogozhnikov, A. Ustyuzhanin, and M. Williams, *LHCb topological trigger reoptimization*, J. Phys. Conf. Ser. **664** (2015) 082025, [arXiv:1510.00572](#).
- [72] LHCb collaboration, R. Aaij *et al.*, *Measurement of the $B_s^0 \rightarrow \mu^+ \mu^-$ branching fraction and effective lifetime and search for $B^0 \rightarrow \mu^+ \mu^-$ decays*, Phys. Rev. Lett. **118** (2017) 191801, [arXiv:1703.05747](#).

Supplemental Material

Prompt-Like Fits

The fit strategy denoted by aic-o and described in detail in Ref. [65] is used in the prompt-like A' search. The $m(\mu^+\mu^-)$ spectrum is scanned in steps of $\sigma[m(\mu^+\mu^-)]/2$ searching for $A' \rightarrow \mu^+\mu^-$ contributions. At each mass, a binned extended maximum likelihood fit is performed, and the profile likelihood is used to determine the p -value and the confidence interval on $n_{\text{ob}}^{A'}[m(A')]$. The prompt-like-search trials factor is obtained using pseudoexperiments. As in Ref. [65], each fit is performed in a $\pm 12.5\sigma[m(\mu^+\mu^-)]$ window around the scan-mass value using bins with widths of $\sigma[m(\mu^+\mu^-)]/20$. Near threshold, the quantity $q(\mu^+\mu^-) \equiv \sqrt{m(\mu^+\mu^-)^2 - 4m(\mu)^2}$ is used instead of the mass since it is easier to model. The confidence intervals are defined using the *bounded likelihood* approach, which involves taking $\Delta \log \mathcal{L}$ relative to zero signal, rather than the best-fit value, if the best-fit signal value is negative. This approach enforces that only physical (nonnegative) upper limits are placed on $n_{\text{ob}}^{A'}[m(A')]$, and prevents defining exclusion regions that are much better than the experimental sensitivity in cases where a large deficit in the background yield is observed.

The signal models are determined at each $m(A')$ using a combination of simulated $A' \rightarrow \mu^+\mu^-$ decays and the widths of the large resonance peaks that are clearly visible in the data. The background models are chosen following the method of Ref. [65]. This method takes as input a large set of potential background components, then performs a data-driven model-selection process whose uncertainty is included in the profile likelihood following Ref. [66]. In this analysis, the set of possible background components includes all Legendre modes with $\ell \leq 10$ at every $m(A')$. Additionally, dedicated background components are included to model the near-threshold turn-on behavior and all sizable known resonance contributions.

The use of 11 Legendre modes adequately describes every double-misidentified peaking background that contributes at a significant level, *e.g.*, $\phi \rightarrow K^+K^-$ and $D \rightarrow K^\pm\pi^\mp$ double misidentified as dimuons, and in the D case misreconstructed as prompt-like, do not require dedicated background components. In mass regions where such complexity is not required, the data-driven model-selection procedure reduces the complexity which increases the sensitivity to a potential signal contribution. As in Ref. [65], all fit regions are transformed onto the interval $[-1, 1]$, where the scan $m(A')$ value maps to zero. After such a transformation, the signal model is (approximately) an even function; therefore, odd Legendre modes are orthogonal to the signal component, which means that the presence of odd modes has minimal impact on the variance of $n_{\text{ob}}^{A'}[m(A')]$. In the prompt-like fits, all odd Legendre modes up to ninth order are included in every background model, while only a subset of the even modes is selected for inclusion in each fit.

Regions in the mass spectrum where large known resonance contributions are observed are vetoed in the prompt-like A' search. Furthermore, the regions near the η' meson and the excited Υ states (beyond the $\Upsilon(4S)$ meson) are treated specially. For example, since it is not possible to distinguish between $A' \rightarrow \mu^+\mu^-$ and $\eta' \rightarrow \mu^+\mu^-$ contributions at $m(\eta')$, the p -values near this mass are ignored. Any excess at $m(\eta')$ is treated as signal when setting the limits on $n_{\text{ob}}^{A'}[m(A')]$, which is conservative in that a $\eta' \rightarrow \mu^+\mu^-$ contribution will weaken the constraints on $A' \rightarrow \mu^+\mu^-$ decays. The same strategy is used near the excited Υ masses. The treatment of all mass regions is summarized in Table 1.

Table 1: Summary of mass regions with special treatment in the prompt-like A' search. In all other mass regions from 214 MeV to 70 GeV, limits are set and the p -values are considered as possible evidence for $A' \rightarrow \mu^+ \mu^-$ decays.

| $m(A')$ Region [MeV] | Resonance(s) | Special Treatment |
|------------------------|---------------------------------|-------------------------------------|
| (524, 571) | η | no search |
| (741, 827) | ω | no search |
| (940, 960) | η' | limits set, but p -values ignored |
| (960, 1100) | ϕ | no search |
| (2700, 3300) | J/ψ | no search |
| (3600, 3800) | $\psi(2S)$ and $\psi(3770)$ | no search |
| (9100, 10600) | $\Upsilon(1S)$ – $\Upsilon(4S)$ | no search |
| (10840, 11040) | excited Υ states | limits set, but p -values ignored |

Long-Lived Fits

The long-lived signal yields are determined from binned extended maximum likelihood fits performed on all long-lived $A' \rightarrow \mu^+ \mu^-$ candidates using the three-dimensional feature space of the dimuon invariant mass, $m(\mu^+ \mu^-)$, the A' decay time, t , and the decay-fit quality, χ_{DF}^2 . As in the prompt-like A' search, a scan is performed in discrete steps of $\sigma[m(\mu^+ \mu^-)]/2$; however, in this case, discrete steps in $\tau(A')$ are also considered. The profile likelihood is again used to obtain the p -values and the confidence intervals on $n_{\text{ob}}^{A'}[m(A'), \tau(A')]$. The binning scheme involves four bins in χ_{DF}^2 : [0,2], [2,4], [4,6], and [6,8]. Eight bins in t are used: [0.2,0.6], [0.6,1.1], [1.1,1.6], [1.6,2.2], [2.2,3.0], [3,5], [5,10], and > 10 ps. The binning scheme used for $m(\mu^+ \mu^-)$ depends on the scan $m(A')$ value, and is chosen such that the majority of the signal falls into a single bin. Signal decays mostly have small χ_{DF}^2 values, with about 50% (80%) of $A' \rightarrow \mu^+ \mu^-$ decays satisfying $\chi_{\text{DF}}^2 < 2$ (4). Background from b -hadron decays populates the small t region and is roughly uniformly distributed in χ_{DF}^2 , whereas background from K_s^0 decays is signal-like in χ_{DF}^2 and roughly uniformly distributed in t . Figure 4 shows the three-dimensional distribution of all long-lived $A' \rightarrow \mu^+ \mu^-$ candidates.

The expected contribution in each bin from photon conversions is derived from the number of candidates rejected by the conversion criterion. As discussed in the Letter, two large control data samples are used to develop and validate the modeling of the b -hadron and K_s^0 contributions. Both contributions are well modeled by the function $\Theta[q(\mu^+ \mu^-) - q_0] \times \{a[q(\mu^+ \mu^-) - q_0] + b[q(\mu^+ \mu^-) - q_0]^2\}$, where q_0 , a , and b are fitted to the data, and Θ denotes the Heaviside step function. While no evidence for t or χ_{DF}^2 dependence is observed for these parameters in either the b -hadron or K_s^0 control sample, all parameters are allowed to vary independently in each $[t, \chi_{\text{DF}}^2]$ region in the fits used in the long-lived A' search.

Figure 6 shows the long-lived $A' \rightarrow \mu^+ \mu^-$ candidates, along with the pull values obtained from fits performed to the data where no signal contributions are included. All of the pulls are in the range $[-2, 2]$. *N.b.*, due to the fact that the background threshold parameters are free to vary in each $[t, \chi_{\text{DF}}^2]$ region, the lowest-mass nonempty bin for each $[t, \chi_{\text{DF}}^2]$ is biased towards a positive pull in the absence of a signal contribution.

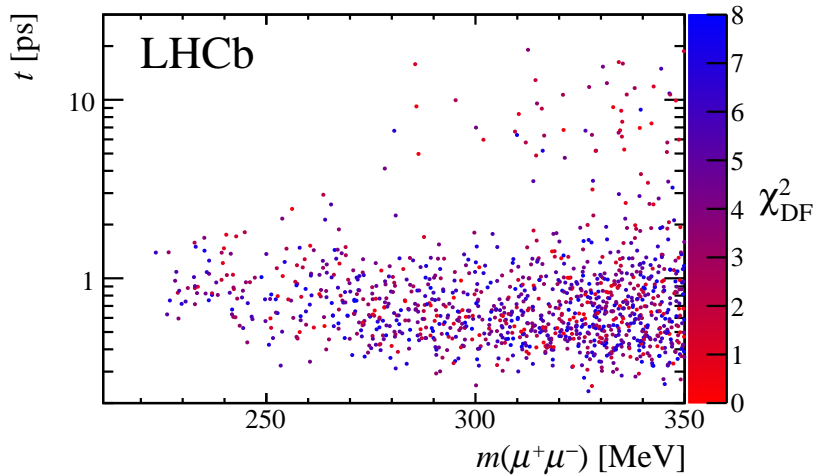


Figure 4: Three-dimensional distribution of χ^2_{DF} versus t versus $m(\mu^+\mu^-)$, which is fit to determine the long-lived signal yields. The data are consistent with being predominantly due to b -hadron decays at small t , and due to K_s^0 decays for large t and $m(\mu^+\mu^-) \gtrsim 280$ MeV. The largest signal-like excess occurs at $m(A') = 239$ MeV and $\tau(A') = 0.86$ ps.

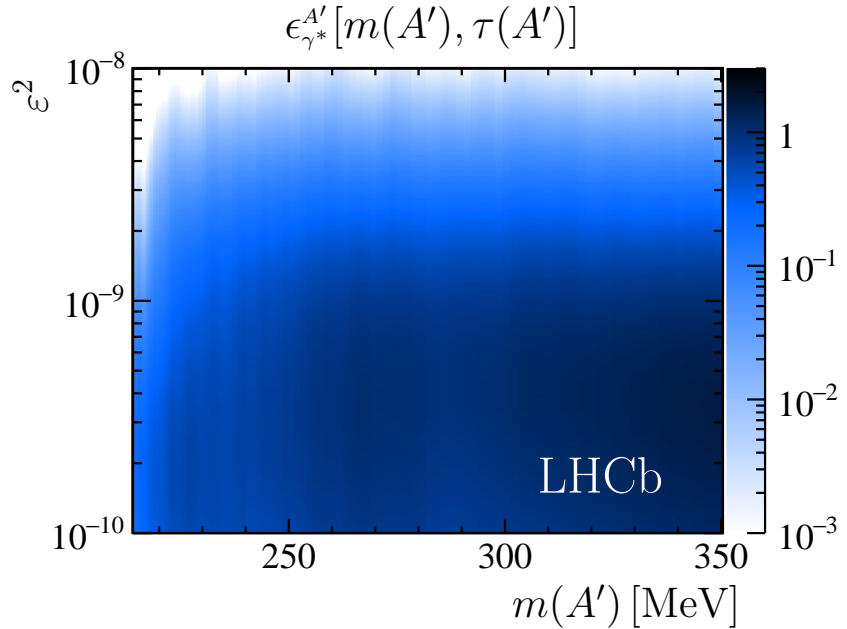


Figure 5: Efficiency ratio $\epsilon_{\gamma^*}^{A'}[m(A'), \tau(A')]$ for long-lived dark photons, integrated over decay time. The sharp decrease at larger values of ε^2 is due to the stringent $\min[\chi^2_{\text{IP}}(\mu^\pm)]$ criterion applied in the 2016 trigger.

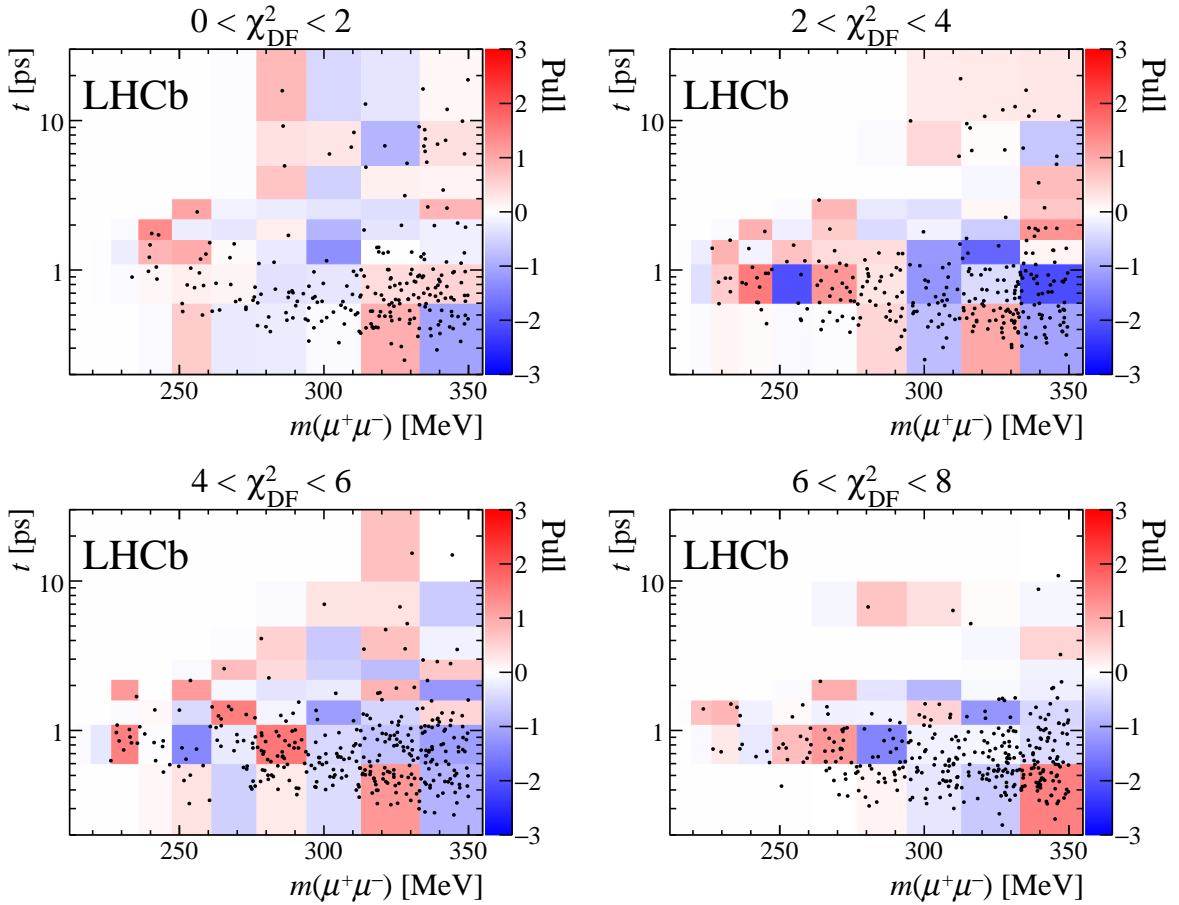


Figure 6: Long-lived $A' \rightarrow \mu^+ \mu^-$ candidates (black points) showing t versus $m(\mu^+ \mu^-)$ in bins of χ^2_{DF} , compared to the pulls from binned fits performed without a signal contribution (color axis). Positive pulls denote an excess of data candidates.

Additional Figures

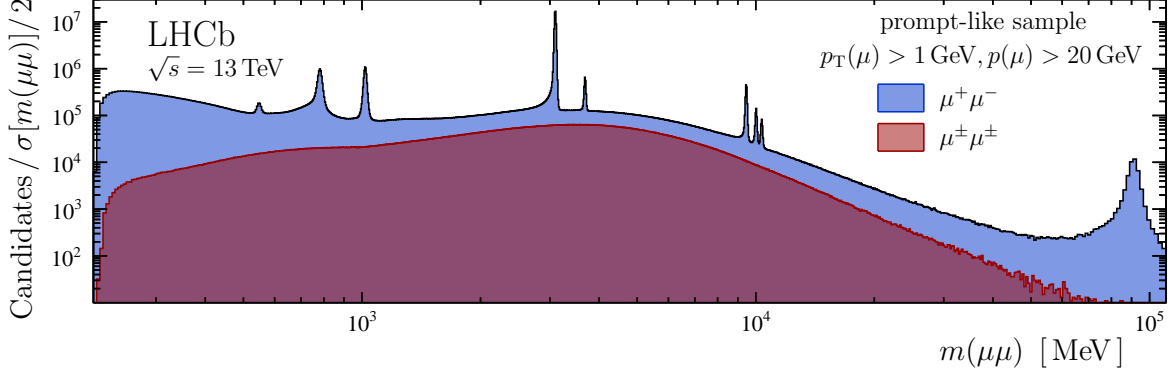


Figure 7: Mass spectrum selected by the prompt-like $A' \rightarrow \mu^+\mu^-$ trigger.

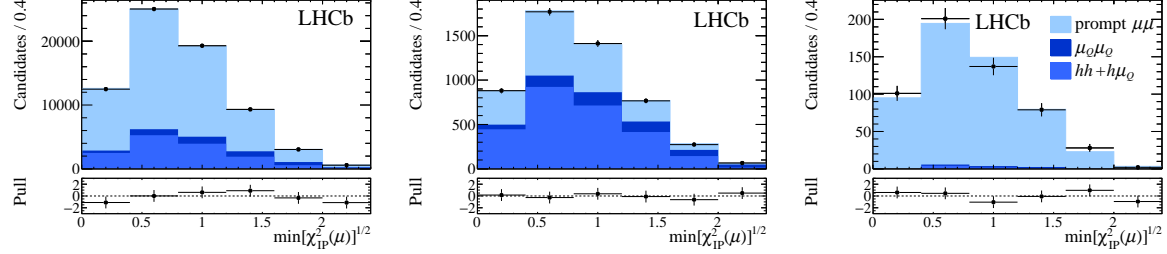


Figure 8: Example $\min[\chi^2_{\text{IP}}(\mu^\pm)]^{1/2}$ distributions with fit results overlaid for prompt-like candidates near (left) $m(A') = 0.5$, (middle) 5, and (right) 50 GeV. The square root of $\min[\chi^2_{\text{IP}}(\mu^\pm)]$ is used in the fits to increase the bin occupancies at large $\min[\chi^2_{\text{IP}}(\mu^\pm)]$ values.

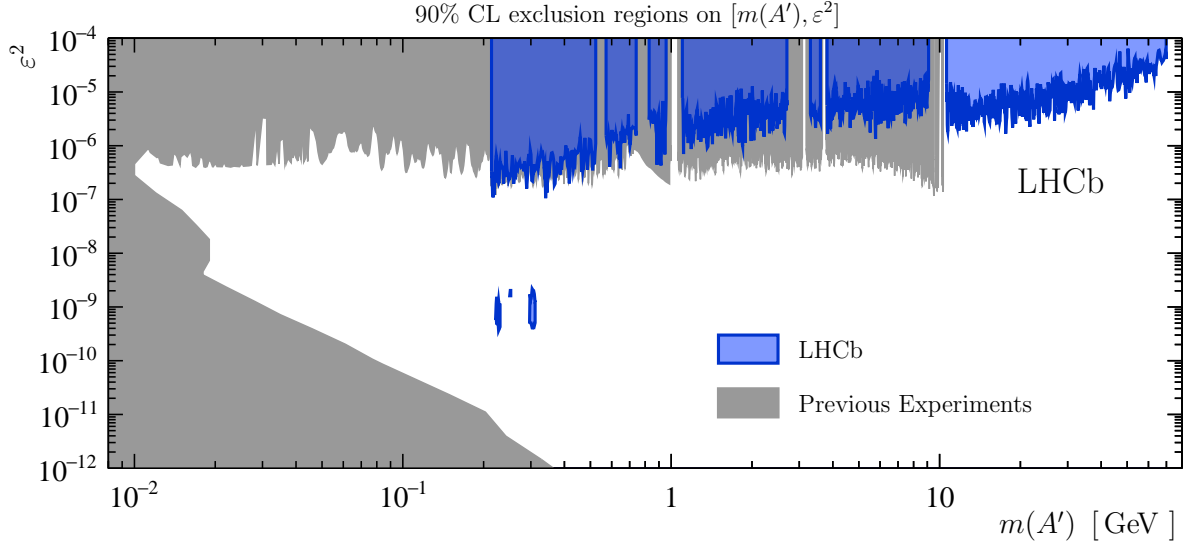


Figure 9: Comparison of the results presented in this Letter to existing constraints from previous experiments (see Ref. [1] for details about previous experiments).

LHCb collaboration

R. Aaij⁴⁰, B. Adeva³⁹, M. Adinolfi⁴⁸, Z. Ajaltouni⁵, S. Akar⁵⁹, J. Albrecht¹⁰, F. Alessio⁴⁰, M. Alexander⁵³, A. Alfonso Albero³⁸, S. Ali⁴³, G. Alkhazov³¹, P. Alvarez Cartelle⁵⁵, A.A. Alves Jr⁵⁹, S. Amato², S. Amerio²³, Y. Amhis⁷, L. An³, L. Anderlini¹⁸, G. Andreassi⁴¹, M. Andreotti^{17,g}, J.E. Andrews⁶⁰, R.B. Appleby⁵⁶, F. Archilli⁴³, P. d'Argent¹², J. Arnau Romeu⁶, A. Artamonov³⁷, M. Artuso⁶¹, E. Aslanides⁶, M. Atzeni⁴², G. Auriemma²⁶, M. Baalouch⁵, I. Babuschkin⁵⁶, S. Bachmann¹², J.J. Back⁵⁰, A. Badalov^{38,m}, C. Baesso⁶², S. Baker⁵⁵, V. Balagura^{7,b}, W. Baldini¹⁷, A. Baranov³⁵, R.J. Barlow⁵⁶, C. Barschel⁴⁰, S. Barsuk⁷, W. Barter⁵⁶, F. Baryshnikov³², V. Batozskaya²⁹, V. Battista⁴¹, A. Bay⁴¹, L. Beauchourt⁴, J. Beddow⁵³, F. Bedeschi²⁴, I. Bediaga¹, A. Beiter⁶¹, L.J. Bel⁴³, N. Beliy⁶³, V. Bellee⁴¹, N. Belloli^{21,i}, K. Belous³⁷, I. Belyaev^{32,40}, E. Ben-Haim⁸, G. Bencivenni¹⁹, S. Benson⁴³, S. Beranek⁹, A. Berezhnoy³³, R. Bernet⁴², D. Berninghoff¹², E. Bertholet⁸, A. Bertolin²³, C. Betancourt⁴², F. Betti¹⁵, M.-O. Bettler⁴⁰, M. van Beuzekom⁴³, Ia. Bezshyiko⁴², S. Bifani⁴⁷, P. Billoir⁸, A. Birnkraut¹⁰, A. Bizzeti^{18,u}, M. Bjørn⁵⁷, T. Blake⁵⁰, F. Blanc⁴¹, S. Blusk⁶¹, V. Bocci²⁶, T. Boettcher⁵⁸, A. Bondar^{36,w}, N. Bondar³¹, I. Bordyuzhin³², S. Borghi⁵⁶, M. Borisjak³⁵, M. Borsato³⁹, F. Bossu⁷, M. Bouabdil⁹, T.J.V. Bowcock⁵⁴, E. Bowen⁴², C. Bozzi^{17,40}, S. Braun¹², T. Britton⁶¹, J. Brodzicka²⁷, D. Brundu¹⁶, E. Buchanan⁴⁸, C. Burr⁵⁶, A. Bursche^{16,f}, J. Buytaert⁴⁰, W. Byczynski⁴⁰, S. Cadeddu¹⁶, H. Cai⁶⁴, R. Calabrese^{17,g}, R. Calladine⁴⁷, M. Calvi^{21,i}, M. Calvo Gomez^{38,m}, A. Camboni^{38,m}, P. Campana¹⁹, D.H. Campora Perez⁴⁰, L. Capriotti⁵⁶, A. Carbone^{15,e}, G. Carboni^{25,j}, R. Cardinale^{20,h}, A. Cardini¹⁶, P. Carniti^{21,i}, L. Carson⁵², K. Carvalho Akiba², G. Casse⁵⁴, L. Cassina²¹, M. Cattaneo⁴⁰, G. Cavallero^{20,40,h}, R. Cenci^{24,t}, D. Chamont⁷, M.G. Chapman⁴⁸, M. Charles⁸, Ph. Charpentier⁴⁰, G. Chatzikonstantinidis⁴⁷, M. Chefdeville⁴, S. Chen¹⁶, S.F. Cheung⁵⁷, S.-G. Chitic⁴⁰, V. Chobanova^{39,40}, M. Chrzaszcz^{42,27}, A. Chubykin³¹, P. Ciambrone¹⁹, X. Cid Vidal³⁹, G. Ciezarek⁴³, P.E.L. Clarke⁵², M. Clemencic⁴⁰, H.V. Cliff⁴⁹, J. Closier⁴⁰, J. Cogan⁶, E. Cogneras⁵, V. Cogoni^{16,f}, L. Cojocariu³⁰, P. Collins⁴⁰, T. Colombo⁴⁰, A. Comerma-Montells¹², A. Contu⁴⁰, A. Cook⁴⁸, G. Coombs⁴⁰, S. Coquereau³⁸, G. Corti⁴⁰, M. Corvo^{17,g}, C.M. Costa Sobral⁵⁰, B. Couturier⁴⁰, G.A. Cowan⁵², D.C. Craik⁵⁸, A. Crocombe⁵⁰, M. Cruz Torres¹, R. Currie⁵², C. D'Ambrosio⁴⁰, F. Da Cunha Marinho², E. Dall'Occo⁴³, J. Dalseno⁴⁸, A. Davis³, O. De Aguiar Francisco⁴⁰, S. De Capua⁵⁶, M. De Cian¹², J.M. De Miranda¹, L. De Paula², M. De Serio^{14,d}, P. De Simone¹⁹, C.T. Dean⁵³, D. Decamp⁴, L. Del Buono⁸, H.-P. Dembinski¹¹, M. Demmer¹⁰, A. Dendek²⁸, D. Derkach³⁵, O. Deschamps⁵, F. Dettori⁵⁴, B. Dey⁶⁵, A. Di Canto⁴⁰, P. Di Nezza¹⁹, H. Dijkstra⁴⁰, F. Dordei⁴⁰, M. Dorigo⁴⁰, A. Dosil Suárez³⁹, L. Douglas⁵³, A. Dovbnya⁴⁵, K. Dreimanis⁵⁴, L. Dufour⁴³, G. Dujany⁸, P. Durante⁴⁰, R. Dzhelyadin³⁷, M. Dziewiecki¹², A. Dziurda⁴⁰, A. Dzyuba³¹, S. Easo⁵¹, M. Ebert⁵², U. Egede⁵⁵, V. Egorychev³², S. Eidelman^{36,w}, S. Eisenhardt⁵², U. Eitschberger¹⁰, R. Ekelhof¹⁰, L. Eklund⁵³, S. Ely⁶¹, S. Esen¹², H.M. Evans⁴⁹, T. Evans⁵⁷, A. Falabella¹⁵, N. Farley⁴⁷, S. Farry⁵⁴, D. Fazzini^{21,i}, L. Federici²⁵, D. Ferguson⁵², G. Fernandez³⁸, P. Fernandez Declara⁴⁰, A. Fernandez Prieto³⁹, F. Ferrari¹⁵, F. Ferreira Rodrigues², M. Ferro-Luzzi⁴⁰, S. Filippov³⁴, R.A. Fini¹⁴, M. Fiorini^{17,g}, M. Firlej²⁸, C. Fitzpatrick⁴¹, T. Fiutowski²⁸, F. Fleuret^{7,b}, K. Fohl⁴⁰, M. Fontana^{16,40}, F. Fontanelli^{20,h}, D.C. Forshaw⁶¹, R. Forty⁴⁰, V. Franco Lima⁵⁴, M. Frank⁴⁰, C. Frei⁴⁰, J. Fu^{22,q}, W. Funk⁴⁰, E. Furfarò^{25,j}, C. Färber⁴⁰, E. Gabriel⁵², A. Gallas Torreira³⁹, D. Galli^{15,e}, S. Gallorini²³, S. Gambetta⁵², M. Gandelman², P. Gandini²², Y. Gao³, L.M. Garcia Martin⁷⁰, J. García Pardiñas³⁹, J. Garra Tico⁴⁹, L. Garrido³⁸, P.J. Garsed⁴⁹, D. Gascon³⁸, C. Gaspar⁴⁰, L. Gavardi¹⁰, G. Gazzoni⁵, D. Gerick¹², E. Gersabeck⁵⁶, M. Gersabeck⁵⁶, T. Gershon⁵⁰, Ph. Ghez⁴, S. Gianì⁴¹, V. Gibson⁴⁹, O.G. Girard⁴¹, L. Giubega³⁰, K. Gizzov⁵², V.V. Gligorov⁸, D. Golubkov³², A. Golutvin⁵⁵, A. Gomes^{1,a}, I.V. Gorelov³³, C. Gotti^{21,i}, E. Govorkova⁴³, J.P. Grabowski¹², R. Graciani Diaz³⁸, L.A. Granado Cardoso⁴⁰, E. Graugés³⁸, E. Graverini⁴²,

G. Graziani¹⁸, A. Grecu³⁰, R. Greim⁹, P. Griffith¹⁶, L. Grillo²¹, L. Gruber⁴⁰,
 B.R. Gruberg Cazon⁵⁷, O. Grünberg⁶⁷, E. Gushchin³⁴, Yu. Guz³⁷, T. Gys⁴⁰, C. Göbel⁶²,
 T. Hadavizadeh⁵⁷, C. Hadjivasilou⁵, G. Haefeli⁴¹, C. Haen⁴⁰, S.C. Haines⁴⁹, B. Hamilton⁶⁰,
 X. Han¹², T.H. Hancock⁵⁷, S. Hansmann-Menzemer¹², N. Harnew⁵⁷, S.T. Harnew⁴⁸, C. Hasse⁴⁰,
 M. Hatch⁴⁰, J. He⁶³, M. Hecker⁵⁵, K. Heinicke¹⁰, A. Heister⁹, K. Hennessy⁵⁴, P. Henrard⁵,
 L. Henry⁷⁰, E. van Herwijnen⁴⁰, M. Heß⁶⁷, A. Hicheur², D. Hill⁵⁷, C. Hombach⁵⁶,
 P.H. Hopchev⁴¹, W. Hu⁶⁵, Z.C. Huard⁵⁹, W. Hulsbergen⁴³, T. Humair⁵⁵, M. Hushchyn³⁵,
 D. Hutchcroft⁵⁴, P. Ibis¹⁰, M. Idzik²⁸, P. Ilten⁵⁸, R. Jacobsson⁴⁰, J. Jalocha⁵⁷, E. Jans⁴³,
 A. Jawahery⁶⁰, F. Jiang³, M. John⁵⁷, D. Johnson⁴⁰, C.R. Jones⁴⁹, C. Joram⁴⁰, B. Jost⁴⁰,
 N. Jurik⁵⁷, S. Kandybei⁴⁵, M. Karacson⁴⁰, J.M. Kariuki⁴⁸, S. Karodia⁵³, N. Kazeev³⁵,
 M. Kecke¹², F. Keizer⁴⁹, M. Kelsey⁶¹, M. Kenzie⁴⁹, T. Ketel⁴⁴, E. Khairullin³⁵, B. Khanji¹²,
 C. Khurewathanakul⁴¹, T. Kirn⁹, S. Klaver⁵⁶, K. Klimaszewski²⁹, T. Klimkovich¹¹, S. Koliev⁴⁶,
 M. Kolpin¹², R. Kopecna¹², P. Koppenburg⁴³, A. Kosmyntseva³², S. Kotriakhova³¹,
 M. Kozeiha⁵, L. Kravchuk³⁴, M. Kreps⁵⁰, F. Kress⁵⁵, P. Krokovny^{36,w}, F. Kruse¹⁰,
 W. Krzemien²⁹, W. Kucewicz^{27,l}, M. Kucharczyk²⁷, V. Kudryavtsev^{36,w}, A.K. Kuonen⁴¹,
 T. Kvaratskheliya^{32,40}, D. Lacarrere⁴⁰, G. Lafferty⁵⁶, A. Lai¹⁶, G. Lanfranchi¹⁹,
 C. Langenbruch⁹, T. Latham⁵⁰, C. Lazzeroni⁴⁷, R. Le Gac⁶, A. Leflat^{33,40}, J. Lefrançois⁷,
 R. Lefèvre⁵, F. Lemaitre⁴⁰, E. Lemos Cid³⁹, O. Leroy⁶, T. Lesiak²⁷, B. Leverington¹², P.-R. Li⁶³,
 T. Li³, Y. Li⁷, Z. Li⁶¹, T. Likhomanenko⁶⁸, R. Lindner⁴⁰, F. Lionetto⁴², V. Lisovskyi⁷, X. Liu³,
 D. Loh⁵⁰, A. Loi¹⁶, I. Longstaff⁵³, J.H. Lopes², D. Lucchesi^{23,o}, M. Lucio Martinez³⁹, H. Luo⁵²,
 A. Lupato²³, E. Luppi^{17,g}, O. Lupton⁴⁰, A. Lusiani²⁴, X. Lyu⁶³, F. Machefert⁷, F. Maciuc³⁰,
 V. Macko⁴¹, P. Mackowiak¹⁰, S. Maddrell-Mander⁴⁸, O. Maev^{31,40}, K. Maguire⁵⁶,
 D. Maisuzenko³¹, M.W. Majewski²⁸, S. Malde⁵⁷, B. Malecki²⁷, A. Malinin⁶⁸, T. Maltsev^{36,w},
 G. Manca^{16,f}, G. Mancinelli⁶, D. Marangotto^{22,q}, J. Maratas^{5,v}, J.F. Marchand⁴, U. Marconi¹⁵,
 C. Marin Benito³⁸, M. Marinangeli⁴¹, P. Marino⁴¹, J. Marks¹², G. Martellotti²⁶, M. Martin⁶,
 M. Martinelli⁴¹, D. Martinez Santos³⁹, F. Martinez Vidal⁷⁰, L.M. Massacrier⁷, A. Massafferri¹,
 R. Matev⁴⁰, A. Mathad⁵⁰, Z. Mathe⁴⁰, C. Matteuzzi²¹, A. Mauri⁴², E. Maurice^{7,b}, B. Maurin⁴¹,
 A. Mazurov⁴⁷, M. McCann^{55,40}, A. McNab⁵⁶, R. McNulty¹³, J.V. Mead⁵⁴, B. Meadows⁵⁹,
 C. Meaux⁶, F. Meier¹⁰, N. Meinert⁶⁷, D. Melnychuk²⁹, M. Merk⁴³, A. Merli^{22,40,q},
 E. Michielin²³, D.A. Milanes⁶⁶, E. Millard⁵⁰, M.-N. Minard⁴, L. Minzoni¹⁷, D.S. Mitzel¹²,
 A. Mogini⁸, J. Molina Rodriguez¹, T. Mombächer¹⁰, I.A. Monroy⁶⁶, S. Monteil⁵,
 M. Morandin²³, M.J. Morello^{24,t}, O. Morgunova⁶⁸, J. Moron²⁸, A.B. Morris⁵², R. Mountain⁶¹,
 F. Muheim⁵², M. Mulder⁴³, D. Müller⁵⁶, J. Müller¹⁰, K. Müller⁴², V. Müller¹⁰, P. Naik⁴⁸,
 T. Nakada⁴¹, R. Nandakumar⁵¹, A. Nandi⁵⁷, I. Nasteva², M. Needham⁵², N. Neri^{22,40},
 S. Neubert¹², N. Neufeld⁴⁰, M. Neuner¹², T.D. Nguyen⁴¹, C. Nguyen-Mau^{41,n}, S. Nieswand⁹,
 R. Niet¹⁰, N. Nikitin³³, T. Nikodem¹², A. Nogay⁶⁸, D.P. O'Hanlon⁵⁰, A. Oblakowska-Mucha²⁸,
 V. Obraztsov³⁷, S. Ogilvy¹⁹, R. Oldeman^{16,f}, C.J.G. Onderwater⁷¹, A. Ossowska²⁷,
 J.M. Otalora Goicochea², P. Owen⁴², A. Oyanguren⁷⁰, P.R. Pais⁴¹, A. Palano¹⁴,
 M. Palutan^{19,40}, A. Papanestis⁵¹, M. Pappagallo^{14,d}, L.L. Pappalardo^{17,g}, W. Parker⁶⁰,
 C. Parkes⁵⁶, G. Passaleva^{18,40}, A. Pastore^{14,d}, M. Patel⁵⁵, C. Patrignani^{15,e}, A. Pearce⁴⁰,
 A. Pellegrino⁴³, G. Penso²⁶, M. Pepe Altarelli⁴⁰, S. Perazzini⁴⁰, P. Perret⁵, L. Pescatore⁴¹,
 K. Petridis⁴⁸, A. Petrolini^{20,h}, A. Petrov⁶⁸, M. Petruzzo^{22,q}, E. Picatoste Olloqui³⁸,
 B. Pietrzyk⁴, M. Pikies²⁷, D. Pinci²⁶, F. Pisani⁴⁰, A. Pistone^{20,h}, A. Piucci¹², V. Placinta³⁰,
 S. Playfer⁵², M. Plo Casasus³⁹, F. Polci⁸, M. Poli Lener¹⁹, A. Poluektov⁵⁰, I. Polyakov⁶¹,
 E. Polycarpo², G.J. Pomery⁴⁸, S. Ponce⁴⁰, A. Popov³⁷, D. Popov^{11,40}, S. Poslavskii³⁷,
 C. Potterat², E. Price⁴⁸, J. Prisciandaro³⁹, C. Prouve⁴⁸, V. Pugatch⁴⁶, A. Puig Navarro⁴²,
 H. Pullen⁵⁷, G. Punzi^{24,p}, W. Qian⁵⁰, R. Quagliani^{7,48}, B. Quintana⁵, B. Rachwal²⁸,
 J.H. Rademacker⁴⁸, M. Rama²⁴, M. Ramos Pernas³⁹, M.S. Rangel², I. Raniuk^{45,†},
 F. Ratnikov³⁵, G. Raven⁴⁴, M. Ravonel Salzgeber⁴⁰, M. Reboud⁴, F. Redi⁵⁵, S. Reichert¹⁰,
 A.C. dos Reis¹, C. Remon Alepuz⁷⁰, V. Renaudin⁷, S. Ricciardi⁵¹, S. Richards⁴⁸, M. Rihl⁴⁰,

K. Rinnert⁵⁴, V. Rives Molina³⁸, P. Robbe⁷, A. Robert⁸, A.B. Rodrigues¹, E. Rodrigues⁵⁹,
 J.A. Rodriguez Lopez⁶⁶, A. Rogozhnikov³⁵, S. Roiser⁴⁰, A. Rollings⁵⁷, V. Romanovskiy³⁷,
 A. Romero Vidal³⁹, J.W. Ronayne¹³, M. Rotondo¹⁹, M.S. Rudolph⁶¹, T. Ruf⁴⁰, P. Ruiz Valls⁷⁰,
 J. Ruiz Vidal⁷⁰, J.J. Saborido Silva³⁹, E. Sadykhov³², N. Sagidova³¹, B. Saitta^{16,f},
 V. Salustino Guimaraes⁶², C. Sanchez Mayordomo⁷⁰, B. Sanmartin Sedes³⁹, R. Santacesaria²⁶,
 C. Santamarina Rios³⁹, M. Santimaria¹⁹, E. Santovetti^{25,j}, G. Sarpis⁵⁶, A. Sarti^{19,k},
 C. Satriano^{26,s}, A. Satta²⁵, D.M. Saunders⁴⁸, D. Savrina^{32,33}, S. Schael⁹, M. Schellenberg¹⁰,
 M. Schiller⁵³, H. Schindler⁴⁰, M. Schmelling¹¹, T. Schmelzer¹⁰, B. Schmidt⁴⁰, O. Schneider⁴¹,
 A. Schopper⁴⁰, H.F. Schreiner⁵⁹, M. Schubiger⁴¹, M.-H. Schune⁷, R. Schwemmer⁴⁰,
 B. Sciascia¹⁹, A. Sciubba^{26,k}, A. Semennikov³², E.S. Sepulveda⁸, A. Sergi⁴⁷, N. Serra⁴²,
 J. Serrano⁶, L. Sestini²³, P. Seyfert⁴⁰, M. Shapkin³⁷, I. Shapoval⁴⁵, Y. Shcheglov³¹, T. Shears⁵⁴,
 L. Shekhtman^{36,w}, V. Shevchenko⁶⁸, B.G. Siddi¹⁷, R. Silva Coutinho⁴², L. Silva de Oliveira²,
 G. Simi^{23,o}, S. Simone^{14,d}, M. Sirendi⁴⁹, N. Skidmore⁴⁸, T. Skwarnicki⁶¹, E. Smith⁵⁵,
 I.T. Smith⁵², J. Smith⁴⁹, M. Smith⁵⁵, I. Soares Lavra¹, M.D. Sokoloff⁵⁹, F.J.P. Soler⁵³,
 B. Souza De Paula², B. Spaan¹⁰, P. Spradlin⁵³, S. Sridharan⁴⁰, F. Stagni⁴⁰, M. Stahl¹²,
 S. Stahl⁴⁰, P. Steffko⁴¹, S. Stefkova⁵⁵, O. Steinkamp⁴², S. Stemmle¹², O. Stenyakin³⁷,
 M. Stepanova³¹, H. Stevens¹⁰, S. Stone⁶¹, B. Storaci⁴², S. Stracka^{24,p}, M.E. Stramaglia⁴¹,
 M. Straticiuc³⁰, U. Straumann⁴², J. Sun³, L. Sun⁶⁴, W. Sutcliffe⁵⁵, K. Swientek²⁸,
 V. Syropoulos⁴⁴, T. Szumlak²⁸, M. Szymanski⁶³, S. T'Jampens⁴, A. Tayduganov⁶,
 T. Tekampe¹⁰, G. Tellarini^{17,g}, F. Teubert⁴⁰, E. Thomas⁴⁰, J. van Tilburg⁴³, M.J. Tilley⁵⁵,
 V. Tisserand⁴, M. Tobin⁴¹, S. Tolk⁴⁹, L. Tomassetti^{17,g}, D. Tonelli²⁴, F. Toriello⁶¹,
 R. Tourinho Jadallah Aoude¹, E. Tournefier⁴, M. Trail⁵³, M.T. Tran⁴¹, M. Tresch⁴²,
 A. Trisovic⁴⁰, A. Tsaregorodtsev⁶, P. Tsopelas⁴³, A. Tully⁴⁹, N. Tuning^{43,40}, A. Ukleja²⁹,
 A. Usachov⁷, A. Ustyuzhanin³⁵, U. Uwer¹², C. Vacca^{16,f}, A. Vagner⁶⁹, V. Vagnoni^{15,40},
 A. Valassi⁴⁰, S. Valat⁴⁰, G. Valenti¹⁵, R. Vazquez Gomez⁴⁰, P. Vazquez Regueiro³⁹, S. Vecchi¹⁷,
 M. van Veghel⁴³, J.J. Velthuis⁴⁸, M. Veltri^{18,r}, G. Veneziano⁵⁷, A. Venkateswaran⁶¹,
 T.A. Verlage⁹, M. Vernet⁵, M. Vesterinen⁵⁷, J.V. Viana Barbosa⁴⁰, B. Viaud⁷, D. Vieira⁶³,
 M. Vieites Diaz³⁹, H. Viemann⁶⁷, X. Vilasis-Cardona^{38,m}, M. Vitti⁴⁹, V. Volkov³³,
 A. Vollhardt⁴², B. Voneki⁴⁰, A. Vorobyev³¹, V. Vorobyev^{36,w}, C. Voß⁹, J.A. de Vries⁴³,
 C. Vázquez Sierra³⁹, R. Waldi⁶⁷, C. Wallace⁵⁰, R. Wallace¹³, J. Walsh²⁴, J. Wang⁶¹,
 D.R. Ward⁴⁹, H.M. Wark⁵⁴, N.K. Watson⁴⁷, D. Websdale⁵⁵, A. Weiden⁴², C. Weisser⁵⁸,
 M. Whitehead⁴⁰, J. Wicht⁵⁰, G. Wilkinson⁵⁷, M. Wilkinson⁶¹, M. Williams⁵⁶, M.P. Williams⁴⁷,
 M. Williams⁵⁸, T. Williams⁴⁷, F.F. Wilson^{51,40}, J. Wimberley⁶⁰, M. Winn⁷, J. Wishahi¹⁰,
 W. Wislicki²⁹, M. Witek²⁷, G. Wormser⁷, S.A. Wotton⁴⁹, K. Wraight⁵³, K. Wyllie⁴⁰, Y. Xie⁶⁵,
 M. Xu⁶⁵, Z. Xu⁴, Z. Yang³, Z. Yang⁶⁰, Y. Yao⁶¹, H. Yin⁶⁵, J. Yu⁶⁵, X. Yuan⁶¹,
 O. Yushchenko³⁷, K.A. Zarebski⁴⁷, M. Zavertyaev^{11,c}, L. Zhang³, Y. Zhang⁷, A. Zhelezov¹²,
 Y. Zheng⁶³, X. Zhu³, V. Zhukov³³, J.B. Zonneveld⁵², S. Zucchelli¹⁵.

¹Centro Brasileiro de Pesquisas Físicas (CBPF), Rio de Janeiro, Brazil

²Universidade Federal do Rio de Janeiro (UFRJ), Rio de Janeiro, Brazil

³Center for High Energy Physics, Tsinghua University, Beijing, China

⁴LAPP, Université Savoie Mont-Blanc, CNRS/IN2P3, Annecy-Le-Vieux, France

⁵Clermont Université, Université Blaise Pascal, CNRS/IN2P3, LPC, Clermont-Ferrand, France

⁶Aix Marseille Univ, CNRS/IN2P3, CPPM, Marseille, France

⁷LAL, Université Paris-Sud, CNRS/IN2P3, Orsay, France

⁸LPNHE, Université Pierre et Marie Curie, Université Paris Diderot, CNRS/IN2P3, Paris, France

⁹I. Physikalisches Institut, RWTH Aachen University, Aachen, Germany

¹⁰Fakultät Physik, Technische Universität Dortmund, Dortmund, Germany

¹¹Max-Planck-Institut für Kernphysik (MPIK), Heidelberg, Germany

¹²Physikalisches Institut, Ruprecht-Karls-Universität Heidelberg, Heidelberg, Germany

¹³School of Physics, University College Dublin, Dublin, Ireland

¹⁴Sezione INFN di Bari, Bari, Italy

- ¹⁵Sezione INFN di Bologna, Bologna, Italy
¹⁶Sezione INFN di Cagliari, Cagliari, Italy
¹⁷Università e INFN, Ferrara, Ferrara, Italy
¹⁸Sezione INFN di Firenze, Firenze, Italy
¹⁹Laboratori Nazionali dell'INFN di Frascati, Frascati, Italy
²⁰Sezione INFN di Genova, Genova, Italy
²¹Università & INFN, Milano-Bicocca, Milano, Italy
²²Sezione di Milano, Milano, Italy
²³Sezione INFN di Padova, Padova, Italy
²⁴Sezione INFN di Pisa, Pisa, Italy
²⁵Sezione INFN di Roma Tor Vergata, Roma, Italy
²⁶Sezione INFN di Roma La Sapienza, Roma, Italy
²⁷Henryk Niewodniczanski Institute of Nuclear Physics Polish Academy of Sciences, Kraków, Poland
²⁸AGH - University of Science and Technology, Faculty of Physics and Applied Computer Science, Kraków, Poland
²⁹National Center for Nuclear Research (NCBJ), Warsaw, Poland
³⁰Horia Hulubei National Institute of Physics and Nuclear Engineering, Bucharest-Magurele, Romania
³¹Petersburg Nuclear Physics Institute (PNPI), Gatchina, Russia
³²Institute of Theoretical and Experimental Physics (ITEP), Moscow, Russia
³³Institute of Nuclear Physics, Moscow State University (SINP MSU), Moscow, Russia
³⁴Institute for Nuclear Research of the Russian Academy of Sciences (INR RAN), Moscow, Russia
³⁵Yandex School of Data Analysis, Moscow, Russia
³⁶Budker Institute of Nuclear Physics (SB RAS), Novosibirsk, Russia
³⁷Institute for High Energy Physics (IHEP), Protvino, Russia
³⁸ICCUB, Universitat de Barcelona, Barcelona, Spain
³⁹Universidad de Santiago de Compostela, Santiago de Compostela, Spain
⁴⁰European Organization for Nuclear Research (CERN), Geneva, Switzerland
⁴¹Institute of Physics, Ecole Polytechnique Fédérale de Lausanne (EPFL), Lausanne, Switzerland
⁴²Physik-Institut, Universität Zürich, Zürich, Switzerland
⁴³Nikhef National Institute for Subatomic Physics, Amsterdam, The Netherlands
⁴⁴Nikhef National Institute for Subatomic Physics and VU University Amsterdam, Amsterdam, The Netherlands
⁴⁵NSC Kharkiv Institute of Physics and Technology (NSC KIPT), Kharkiv, Ukraine
⁴⁶Institute for Nuclear Research of the National Academy of Sciences (KINR), Kyiv, Ukraine
⁴⁷University of Birmingham, Birmingham, United Kingdom
⁴⁸H.H. Wills Physics Laboratory, University of Bristol, Bristol, United Kingdom
⁴⁹Cavendish Laboratory, University of Cambridge, Cambridge, United Kingdom
⁵⁰Department of Physics, University of Warwick, Coventry, United Kingdom
⁵¹STFC Rutherford Appleton Laboratory, Didcot, United Kingdom
⁵²School of Physics and Astronomy, University of Edinburgh, Edinburgh, United Kingdom
⁵³School of Physics and Astronomy, University of Glasgow, Glasgow, United Kingdom
⁵⁴Oliver Lodge Laboratory, University of Liverpool, Liverpool, United Kingdom
⁵⁵Imperial College London, London, United Kingdom
⁵⁶School of Physics and Astronomy, University of Manchester, Manchester, United Kingdom
⁵⁷Department of Physics, University of Oxford, Oxford, United Kingdom
⁵⁸Massachusetts Institute of Technology, Cambridge, MA, United States
⁵⁹University of Cincinnati, Cincinnati, OH, United States
⁶⁰University of Maryland, College Park, MD, United States
⁶¹Syracuse University, Syracuse, NY, United States
⁶²Pontifícia Universidade Católica do Rio de Janeiro (PUC-Rio), Rio de Janeiro, Brazil, associated to ²
⁶³University of Chinese Academy of Sciences, Beijing, China, associated to ³
⁶⁴School of Physics and Technology, Wuhan University, Wuhan, China, associated to ³
⁶⁵Institute of Particle Physics, Central China Normal University, Wuhan, Hubei, China, associated to ³
⁶⁶Departamento de Física, Universidad Nacional de Colombia, Bogota, Colombia, associated to ⁸
⁶⁷Institut für Physik, Universität Rostock, Rostock, Germany, associated to ¹²
⁶⁸National Research Centre Kurchatov Institute, Moscow, Russia, associated to ³²

⁶⁹*National Research Tomsk Polytechnic University, Tomsk, Russia, associated to* ³²

⁷⁰*Instituto de Fisica Corpuscular, Centro Mixto Universidad de Valencia - CSIC, Valencia, Spain, associated to* ³⁸

⁷¹*Van Swinderen Institute, University of Groningen, Groningen, The Netherlands, associated to* ⁴³

^a*Universidade Federal do Triângulo Mineiro (UFTM), Uberaba-MG, Brazil*

^b*Laboratoire Leprince-Ringuet, Palaiseau, France*

^c*P.N. Lebedev Physical Institute, Russian Academy of Science (LPI RAS), Moscow, Russia*

^d*Università di Bari, Bari, Italy*

^e*Università di Bologna, Bologna, Italy*

^f*Università di Cagliari, Cagliari, Italy*

^g*Università di Ferrara, Ferrara, Italy*

^h*Università di Genova, Genova, Italy*

ⁱ*Università di Milano Bicocca, Milano, Italy*

^j*Università di Roma Tor Vergata, Roma, Italy*

^k*Università di Roma La Sapienza, Roma, Italy*

^l*AGH - University of Science and Technology, Faculty of Computer Science, Electronics and Telecommunications, Kraków, Poland*

^m*LIFAELS, La Salle, Universitat Ramon Llull, Barcelona, Spain*

ⁿ*Hanoi University of Science, Hanoi, Viet Nam*

^o*Università di Padova, Padova, Italy*

^p*Università di Pisa, Pisa, Italy*

^q*Università degli Studi di Milano, Milano, Italy*

^r*Università di Urbino, Urbino, Italy*

^s*Università della Basilicata, Potenza, Italy*

^t*Scuola Normale Superiore, Pisa, Italy*

^u*Università di Modena e Reggio Emilia, Modena, Italy*

^v*Iligan Institute of Technology (IIT), Iligan, Philippines*

^w*Novosibirsk State University, Novosibirsk, Russia*

[†]*Deceased*